Supporting Information

Fe_3O_4/FeNi Embedded Nanostructure and Its Kinetic Law for Selective Catalytic Reduction of *p*-Nitrophenyl Compounds

Dandan Wu,† Yanqiao Zhang,† Ming Wen, Hao Fang and Qingsheng Wu*

School of Chemical Science and Engineering, Shanghai Key Laboratory of Chemical Assessment and Sustainability, Tongji University, 1239 Siping Road, Shanghai 200092, R. P. China.

Corresponding Authors

*Ming Wen: E-mail: m_wen@tongji.edu.cn.

1. The Supplement of Experimental Section

1.1. Synthesis of amorphous FeNi 1D nanostructure

The amorphous FeNi alloy catalyst was also prepared through controlling-growth-reduction process in a solvothermal reaction system. The typical synthesis process is described as follows: ferric oxalate aqueous solution (2.4 mL, 7.5 mM) was mixed with nickel acetate triethylene glycol solution (0.6 mL, 30 mM) in a Teflon-lined stainless steel autoclave at room temperature. Then, 18 mL triethylene glycol was injected, followed by ultrasonic treatment for 20 min. The reaction system was sealed and heated at 200°C for 12 h with a heating rate of 1 °C min^{-1}. After the reaction cooled to room temperature, the product was collected by centrifuge. The as-synthesized amorphous FeNi alloy catalyst were alternately washed by ethanol and deionized water three times, then dried in a vacuum oven 60 °C for 4 hours for further characterizations.

1.2. Synthesis of Fe_3O_4 1D nanostructure

The Fe_3O_4 catalyst was prepared through controlling-growth process in a solvothermal reaction system. The typical synthesis process is described as follows: ferric oxalate aqueous solution (4.8 mL, 7.5 mM) was added in a Teflon-lined stainless steel autoclave at room temperature. Then, 16 mL ethylene glycol was injected, followed by ultrasonic treatment for 20 min. The reaction system was sealed and heated at 180°C for 2 h with a heating rate of 1 °C min^{-1}. After the reaction cooled to room temperature, the product was collected by centrifuge. The as-synthesized Fe_3O_4 catalyst were alternately washed by ethanol and deionized water three times, then dried in a vacuum oven 60 °C for 4 hours for further characterizations.

1.3. Synthesis of Fe_3O_4/FeNi NPs, Fe_2O_3/FeNi NPs and amorphous FeNi NPs

Following the analogous synthetic process of Fe_3O_4 1D nanostructure to obtain the Fe_3O_4 NPs catalyst by increasing the heating rate to 5 °C min^{-1} and Fe_2O_3 NPs were prepared by calcining Fe_3O_4 NPs in oxygen at 500 °C for 2 h. Then the prepared

Fe_3O_4 NPs and Fe_2O_3 NPs were used to synthesize Fe_3O_4/FeNi and Fe_2O_3/FeNi nanocomposites, respectively. The typical synthesis process is described as follows: 20 mL $NaBH_4$ aqueous solution (5 mM) was added in the mixture solution with 4.8 mg Fe_3O_4 NPs or 3.5 mg Fe_2O_3 NPs, $NiCl_2$ (25 mL, 5 mM) and $FeCl_2$ (25 mL, 5 mM) under magnetic stirring within 20 min, the final precipitate was filtered, washed thoroughly with deionized water and ethanol, and then dried at 60 °C for 24 h. When without Fe_3O_4 and Fe_2O_3 NPs, amorphous FeNi NPs can be obtained.

2. Results and Discussion

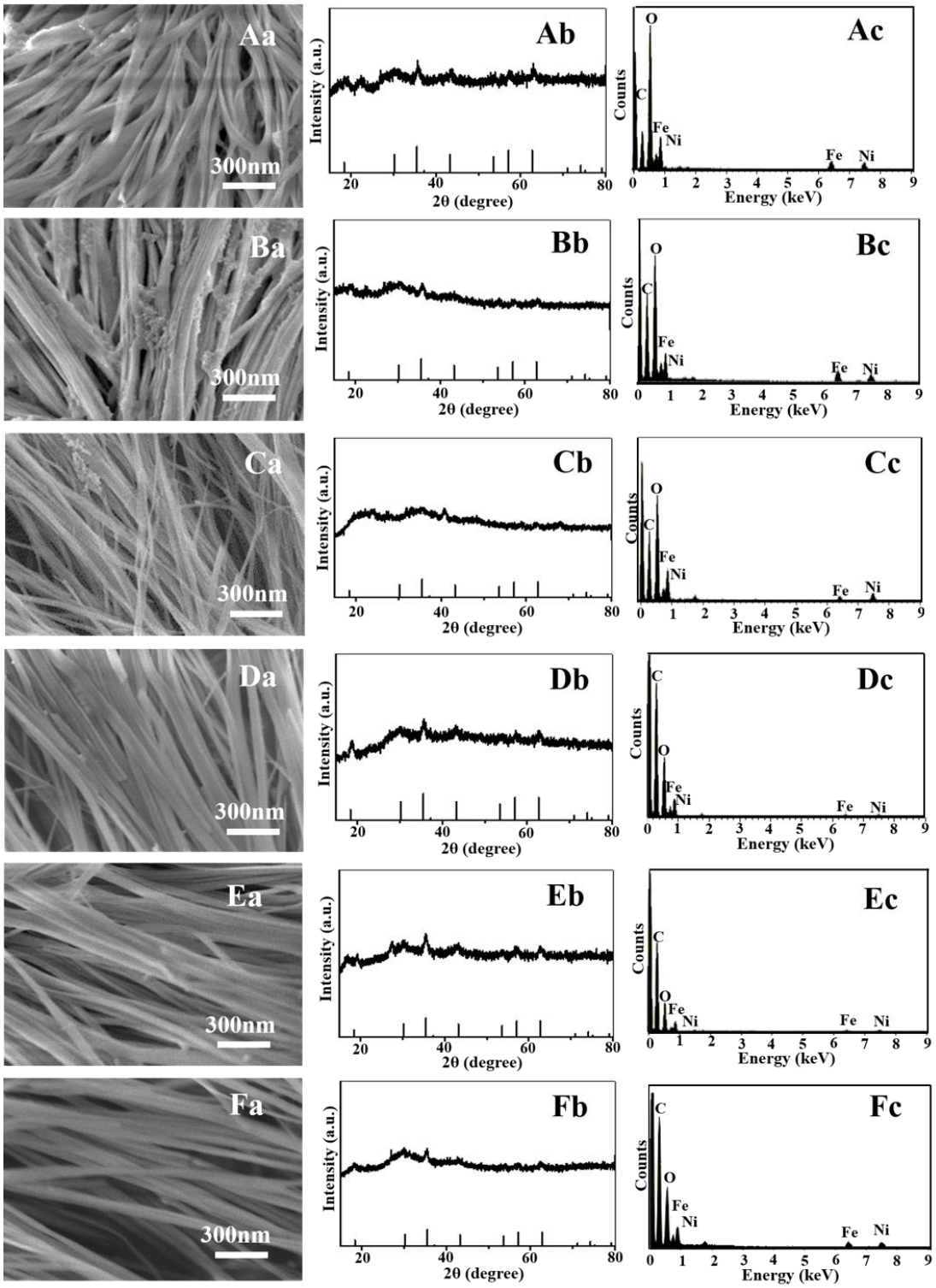

Figure S1. (a) SEM images, (b) XRD patterns, and (c) EDS analysis of Fe_3O_4/FeNi embedded-structured nanocomposite with different FeNi content prepared by different synthesis time: (A) 3h; (B) 6h; (C)9h; (D) 12h; (E) 15h; (F) 18h.

As shown in Figure S1, synthesis time has little effect on the morphology of the Fe_3O_4/FeNi nanocomposite, due to its morphology is mainly controlled by the heating rate, which has been clarified in Scheme 1A (see main text). However, by the EDS analysis we can clearly see that, when the synthesis time less than 12h, the content of oxygen in the as-synthesized samples decreases with the synthesis time, thus revealing the increase of FeNi alloy content. Meanwhile further prolonging the time, the content of FeNi cannot be increased. In addition, as the amorphous phase of FeNi alloy, all the XRD patterns present no distinct peaks of FeNi alloy in as-synthesized samples but only the peaks at 18.3° (111), 30.1° (220) and 35.5° (311) of Fe_3O_4 (JCPDS No. 65-3107).

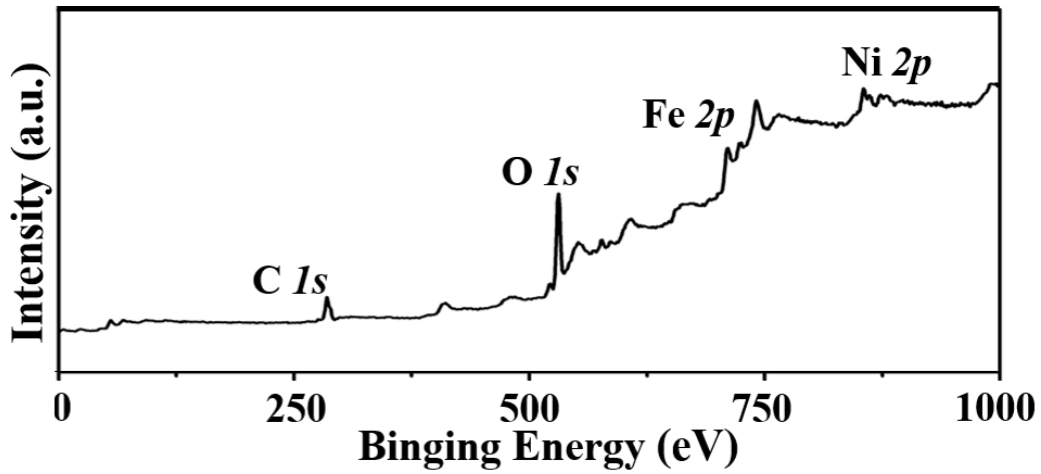

Figure S2. XPS analysis of Fe_3O_4/FeNi nanocomposite

XPS was performed to acquire the valence information of as-designed catalyst and the full spectrum was plotted in Figure S2. In the full spectrum, C *1s*, O *1s*, Fe *2p* and Ni *2p* peaks can be found in the binding energy region from 0 to 1000 eV.

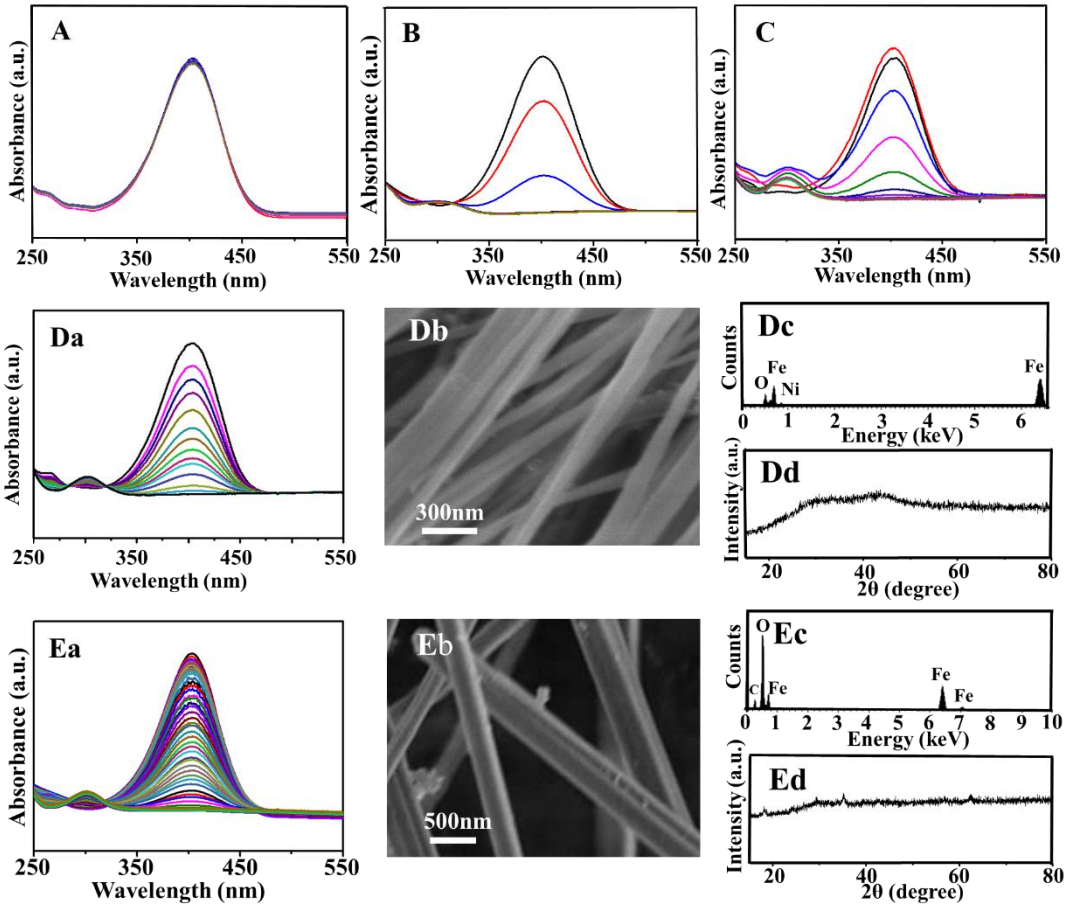

Figure S3. UV-vis spectra for the reduction of *p*-nitrophenol without catalyst (A), and catalyzed by Fe_3O_4/FeNi nanocomposite (B), annealed Fe_3O_4/FeNi nanocomposite (C); (a) UV-vis spectra, (b) SEM images, (c) EDS analysis and (d) XRD patterns of amorphous FeNi alloy (D) and Fe_3O_4 (E).

The spectra of blank experiment were presented in Figure S3A, which show the UV-vis spectra of the hydrogenation reduction of *p*-NPCs at room temperature and ambient atmosphere by employing excess $NaBH_4$ without any catalysts in the reaction. The absorption peak at 400 nm represents *p*-NPCs, and the peak intensity remains unchanged over time and shows a series of overlapped spectra, indicating the reaction doesn't take place without catalyst involving in the reaction.

The UV-Vis adsorption spectra for the reduction of *p*-nitrophenol catalyzed by Fe_3O_4/FeNi nanocomposite, the annealed nanocomposite, amorphous FeNi alloy and Fe_3O_4 are exhibited in Figure S3B, S3C, S3Da and S3Ea, respectively. In Figure S3B, the peak of *p*-nitrophenol decreased immediately and the reaction finished in seconds.

Meanwhile, the peak at 300 nm increased. But as shown in Figure S3C ~ 3Ea, the peak at 400 nm need a longer time to decrease completely. It demonstrates that Fe_3O_4/FeNi nanocomposite catalyst exert higher activity than the other three. Also we can clearly see that the catalytic activity of annealed Fe_3O_4/FeNi embedded nanocomposite better than that of amorphous FeNi alloy, while Fe_3O_4 just shows very weak catalytic activity.

The morphology characterization and structure analysis of amorphous FeNi alloy and Fe_3O_4 are also presented. It can be clearly observed that both amorphous FeNi alloy and Fe_3O_4 have 1D morphology in SEM images (Figure S3Db and Figure S3Eb). The EDS analysis performed separately on amorphous FeNi alloy (Figure S3Dc) and Fe_3O_4 (Figure S3Ec) prove that both of them contain Fe, Ni and O. And the oxygen content of Fe_3O_4 is much higher than FeNi alloy, certifying the formation of Fe_3O_4 and FeNi. The XRD pattern of amorphous FeNi alloy (Figure S3Dd) presents one broad peak at 45° corresponding to fcc structure with a random crystalline orientation, confirming the chemical disorder amorphous structure. However, in Figure S3Ed the sharp peaks at 18.3° (111), 30.1° (220) and 35.5° (311) can be indexed to Fe_3O_4 (JCPDS No. 65-3107).

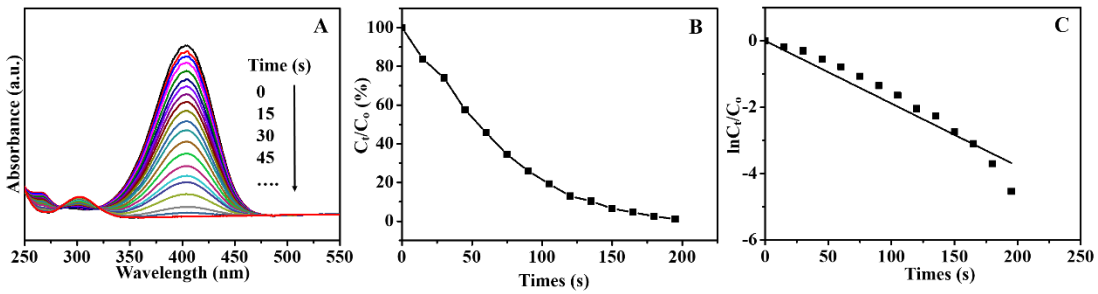

Figure S4. UV-vis spectra (A), plots of C_t/C_0 (B) and $\ln(C_t/C_0)$ (C) vs time for the catalyst prepared by mixing 1D Fe_3O_4 and FeNi nanoalloys directly.

To further prove the advantage of the embedded structure, the contrast catalysts by mixing 1D Fe_3O_4 and FeNi nanoalloys directly were prepared and the catalytic activity of selectively reducing *p*-nitrophenol are shown in Figure S4.

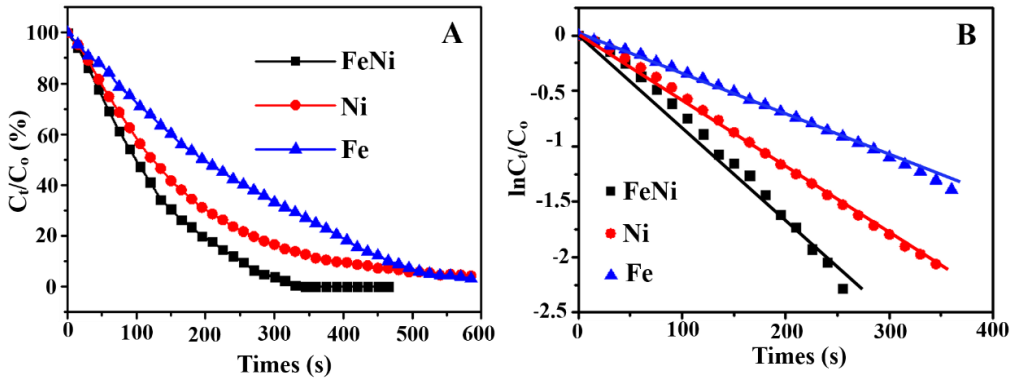

Figure S5. Plots of (A) C_t/C_0 and (B) $\ln(C_t/C_0)$ vs time for the reduction of *p*-nitrophenol catalysed by FeNi, Ni and Fe NPs

To confirm which metal is the active site, Fe, Ni, and FeNi NPs have been synthesized and compared, as shown in Figure S5, the catalytic activity of FeNi NPs for the reduction of *p*-nitrophenol is obviously better than that of others.

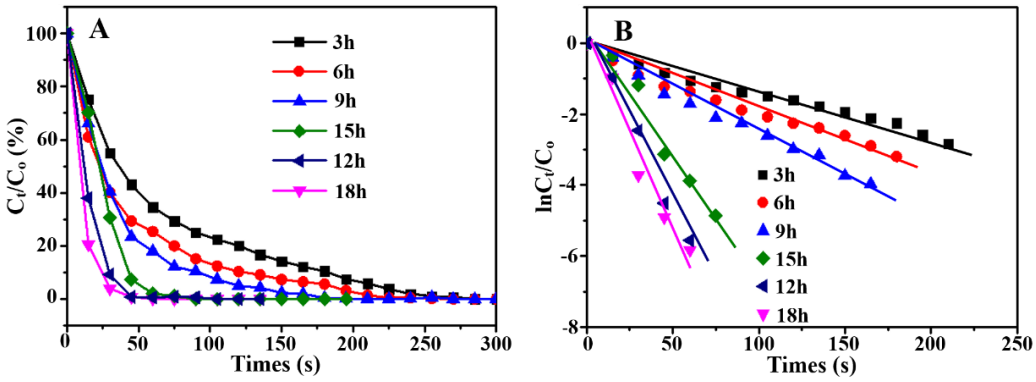

Figure S6. Plots of (A) C_t/C_0 and (B) $\ln(C_t/C_0)$ vs time for the reduction of *p*-nitrophenol catalyzed by the Fe_3O_4/FeNi nanocomposite with different FeNi content prepared by different synthesis time.

Figure S6 shows the normalized data of C_t/C_0 and $\ln(C_t/C_0)$ vs time for the reduction of *p*-NPCs catalyzed by the Fe_3O_4/FeNi nanocomposite with different FeNi content which were prepared by controlling the synthesis time. As shown, when the synthesis time is 12h the catalytic activity of the obtained catalyst reached the best, while further prolonging the time the catalytic activity cannot be improved obviously because of no increase of FeNi content which can be informed by Figure S1.

Table S1. Catalytic performances of different nanocatalysts for the reduction of *p*-nitrophenol.

Catalysts	[*p*-nitrophenol] (mmol/L)	[$NaBH_4$] (mmol/L)	[catalyst] (mg/mL)	Rate constants (min^{-1})	Ref.
Pd	0.1	10	2.12	24.42	(1)
Pd/Au@g-C_3N_4-N	0.7	70	12.5	0.7907	(2)
Au/g-C_3N_4	0.07	4	20	0.356	(3)
Ag/g-C_3N_4	0.1	6	100	15.7	(4)
$NiCo_2$	0.10	60	100	0.07348	(5)
RGO/Ni	0.1	10	65	0.01482	(6)
$Cu_{60}Ni_{40}$−CeO_2	0.1	10	500	9.928	(7)
MoS_2/PMMT	0.12	72	1000	0.723	(8)
3D-NGF	0.077	7.7	58	0.2391	(9)
Fe_3O_4/FeNi	0.067	66.7	100	6.534	This work

Table S1 summaries the catalytic performance comparison of 1D Fe_3O_4/FeNi embedded-structured nanocatalyst with other reported catalysts for the reduction of *p*-nitrophenol. It can be clearly observed that Fe_3O_4/FeNi embedded-structured nanocatalyst presents outstanding catalytic activity than other non-noble-metals catalysts, demonstrating its applications to the recyclable catalyst for efficient and selective reduction of *p*- nitrophenol to *p*-aminophenol.

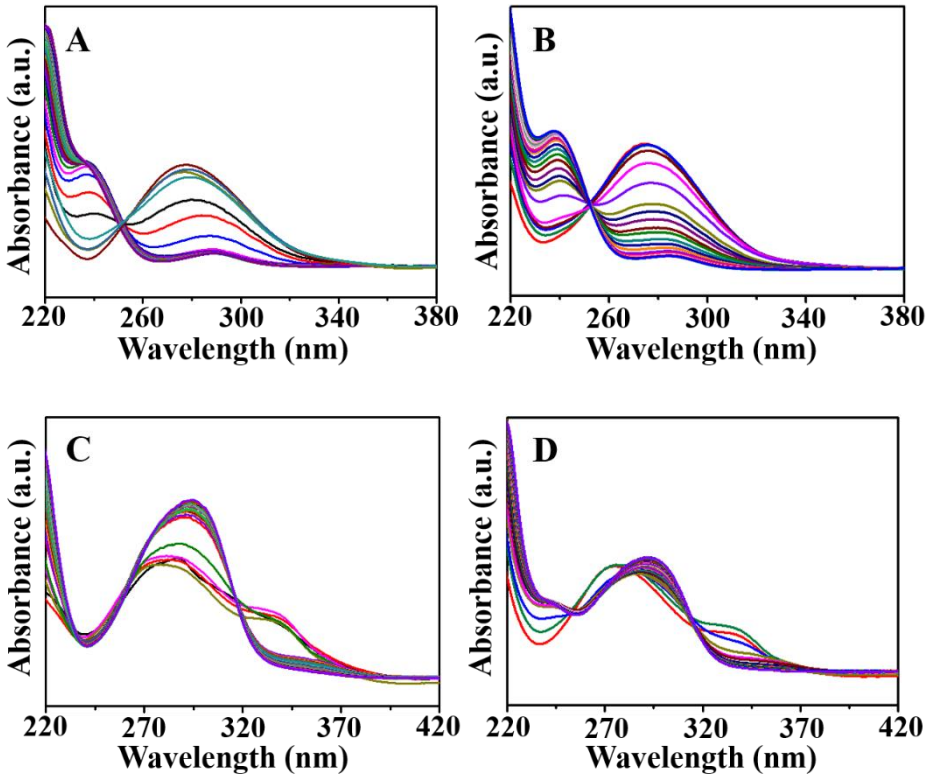

Figure S7. UV-V is spectra of Fe_3O_4/FeNi embedded-structured nanocomposite catalyze different *p*-NPCs: (A) *p*-nitrotoluene; (B) *p*-nitroacetophenone; (C) *p*-nitrobenzaldehyde. (D) UV-Vis spectra of *p*-nitrobenzaldehyde catalyzed by amorphous FeNi alloy.

Figure S7A-S7C show the UV-Vis spectra of Fe_3O_4/FeNi embedded-structured nanocomposite catalyzing different *p*-NPCs. We can clearly see that when *p*-nitrotoluene as catalytic substrate (Figure S7A), the catalytic activity of Fe_3O_4/FeNi embedded-structured nanocomposite is better than *p*-nitroacetophenone as substrate (Figure S7B), while *p*-nitrobenzaldehyde as substrate (Figure S7C) the nanocatalyst just shows very weak catalytic activity. As contrast, when *p*-nitrobenzaldehyde as substrate and catalyzed by amorphous FeNi alloy (Figure S7D), it exhibits no activity in the catalysis. Meanwhile the concentration of *p*-nitrobenzaldehyde is constant without any decrease and shows a series of overlapped spectra. So the Fe_3O_4 nanophase can promote the catalytic activity of amorphous FeNi alloy and the facilitation could be further enhanced when the para group in the nitrophenyl compounds is electron-donating group.

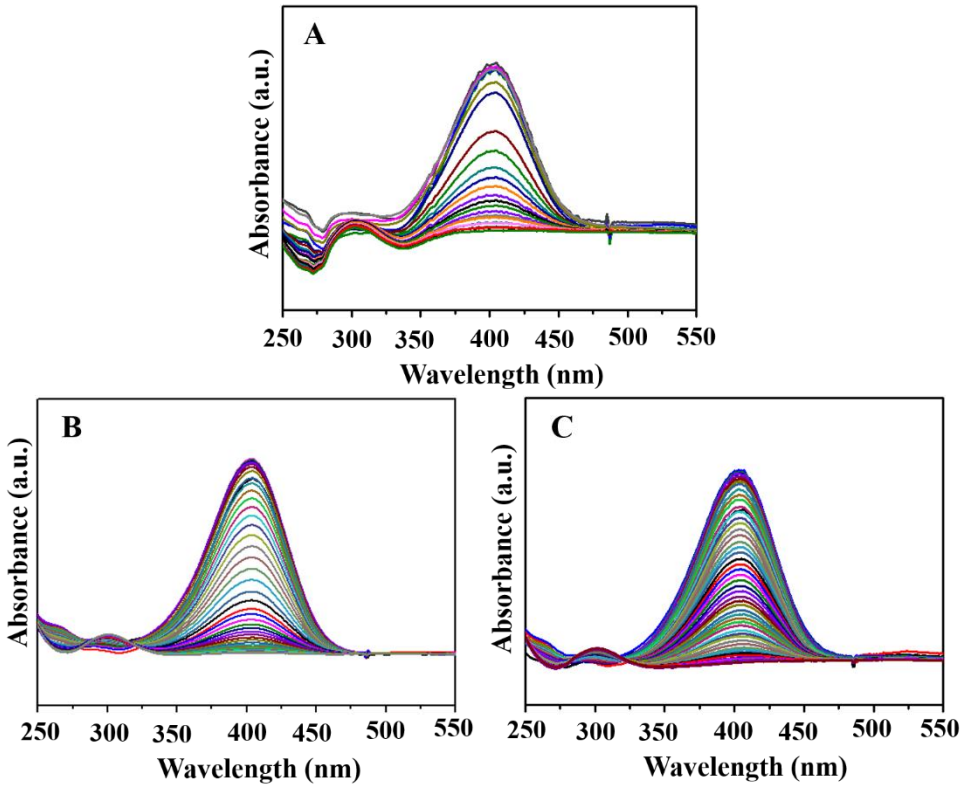

Figure S8. UV-vis spectra for the reduction of *p*-nitrophenol catalyzed by Fe_3O_4/FeNi NPs (A), FeNi NPs (B) and Fe_2O_3/FeNi NPs (C).

In order to clear the role of Fe_3O_4 nanophase, we evaluate the reaction activity catalyzed by as-prepared amorphous FeNi NPs, Fe_2O_3/FeNi NPs and Fe_3O_4/FeNi NPs. In Figure S8, we can clearly see that when Fe_3O_4/FeNi nanocomposite was used as catalyst the characteristic peak at 400 nm of *p*-nitrophenol needed a shorter time to decrease completely than the other two, indicating the Fe_3O_4/FeNi nanocomposite gets the highest activity for the reduction of *p*-nitrophenol. Therefore, Fe_3O_4 can efficiently promote the activity of FeNi in Fe_3O_4/FeNi embedded-structured catalyst.

Table S2. Reaction rate constants in different cycles of Fe_3O_4/FeNi nanocomposite, annealed Fe_3O_4/FeNi nanocomposite and amorphous FeNi alloy as catalysts.

No. of cycles	Reaction rate constants k (s^{-1})		
	Fe_3O_4/FeNi nanocomposite	Annealed Fe_3O_4/FeNi nanocomposite	amorphous FeNi alloy
1	0.0815	0.0797	0.0370
2	0.0979	0.0443	0.0115
3	0.1022	0.0217	0.0226
4	0.1089	0.0096	0.0128
5	0.0856		0.0109
6	0.1014		
7	0.1022		
8	0.1015		
9	0.0999		
10	0.0818		
11	0.0874		
12	0.0773		
13	0.0845		
14	0.0752		
15	0.0684		
16	0.0538		
17	0.0584		
18	0.0552		
19	0.0493		
20	0.0307		

Table S2 summaries the reaction rate constants of different cycles for Fe_3O_4/FeNi nanocomposite, annealed Fe_3O_4/FeNi nanocomposite and amorphous FeNi alloy as catalysts. The catalytic activity of Fe_3O_4/FeNi nanocomposite could keep over 20 times for the reduction of *p*-nitrophenol and the reaction rate constants only slightly changed during the 20 cycles. As contrast, the reaction rate constants of annealed Fe_3O_4/FeNi nanocomposite and amorphous FeNi alloy drop drastically after the 4th cycle.

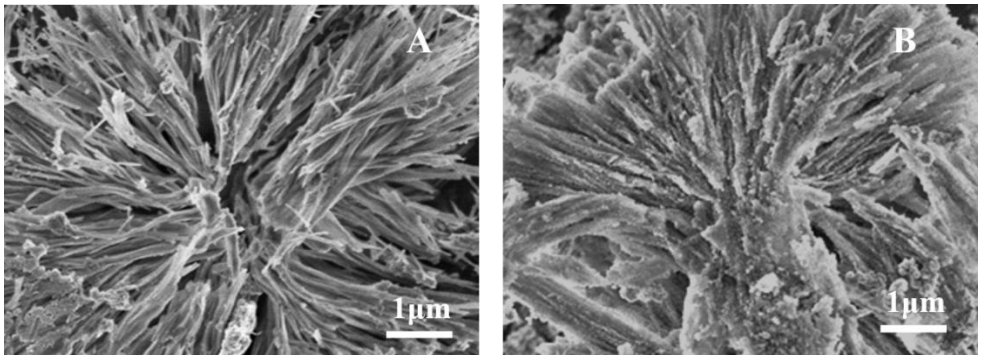

Figure S9. SEM images of Fe_3O_4/FeNi embedded-structured nanocomposite after the 10th (A) and 20th (B) catalytic reduction of *p*-nitrophenol.

Figure S9 shows the monitored SEM images after 10 and 20 catalytic cycles of Fe_3O_4/FeNi embedded-structured nanocomposite, which can be used to further understand the structure stability. It can be clearly seen that Fe_3O_4/FeNi composite maintain the original structure at the 10th cycle basically and appear slight agglomeration after 20 cycles.

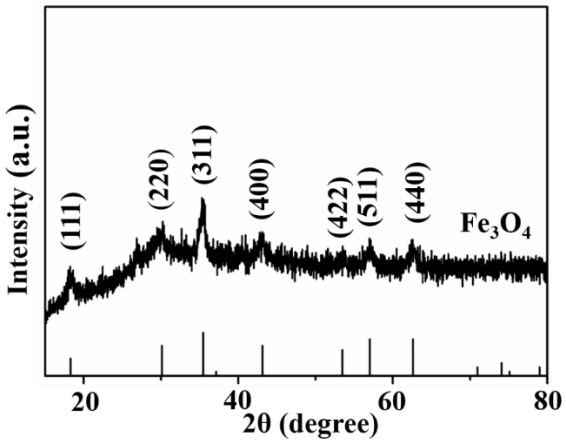

Figure S10. XRD patterns of Fe_3O_4/FeNi embedded-structured nanocomposite after the 20th catalytic reduction of *p*-nitrophenol.

The XRD of Fe_3O_4/FeNi embedded-structured nanocatalyst after 20 cycles was measured to further confirm whether the phase has changed and is shown in Figure S10. We can clearly see that no distinct peaks of FeNi alloy can be observed besides the peaks at 18.3° (111), 30.1° (220) and 35.5° (311) of Fe_3O_4 (JCPDS No. 65-3107), which is consistent with the fresh unused catalyst.

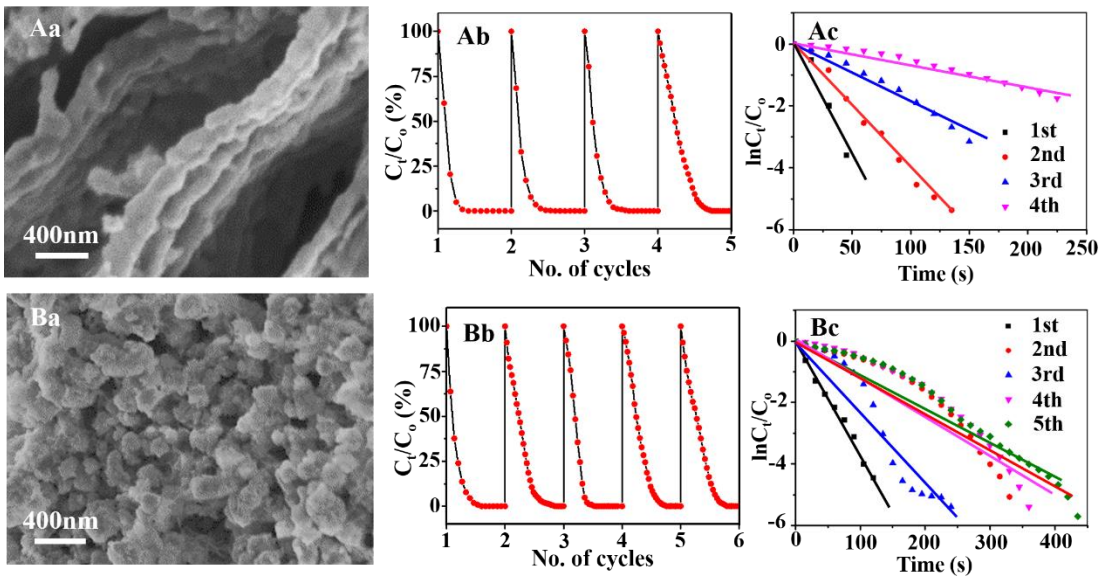

Figure S11. (a) SEM images, (b) Catalytic cycles of the reduction of *p*-nitrophenol and (c) Plots of $\ln(C_t/C_0)$ vs time of annealed Fe_3O_4/FeNi nanocomposite (A) and amorphous FeNi alloy (B).

The lifetime of annealed Fe_3O_4/FeNi nanocomposite and amorphous FeNi alloy were evaluated by successive catalytic tests over 4 and 5 times, respectively. To obtain the catalytic activity data, normalized C_t/C_0 and $\ln(C_t/C_0)$ vs time of each cycle were plotted in Figure S11 and the rate constants of each cycle were calculated and gathered in Table S2. By the catalytic activity data, we can clearly observe that although the morphology of the annealed Fe_3O_4/FeNi composite without apparent agglomeration, it shows much lower catalytic activity than Fe_3O_4/FeNi composite after 4 cycles, indicating excellent catalytic stability come from amorphous FeNi rather than crystalline FeNi. As contrast, the activity decay of amorphous FeNi alloy at the 5th cycle. Meanwhile the SEM image shows a quite easy agglomeration and eventually leads to the catalyst invalid, indicating the embedded-structure of Fe_3O_4/FeNi provides an effective way to construct high-stability performance catalyst.

REFERENCES

[1] Mei, Y.; Lu, Y.; Polzer, F.; Ballauff, M. Catalytic Activity of Palladium Nanoparticles Encapsulated in Spherical Polyelectrolyte Brushes and Core-Shell Microgels. *Chem. Mater.* **2007**, *19*, 1062-1069.

[2] Fang, W.; Deng, Y. C.; Tang, L.; Zeng, G. M.; Zhou, Y. Y.; Xie, X.; Wang, J. J.; Wang, Y.; Wang, J. J. Synthesis of Pd/Au Bimetallic Nanoparticle-Loaded Ultrathin Graphitic Carbon Nitride Nanosheets for Highly Efficient Catalytic Reduction of p-nitrophenol. *J. Colloid Interface Sci.* **2017**, *490*, 834-843.

[3] Fu, Y. S.; Huang, T.; Jia, B. Q.; Zhu, J. W.; Wang, X. Reduction of Nitrophenols to Aminophenols under Concerted Catalysis by Au/g-C_3N_4 Contact System. *Appl. Catal. B: Environ.* **2017**, *202*, 430-437.

[4] Wang, X.; Tan, F. T.; Wang, W.; Qiao, X. L.; Qiu, X. L.; Chen, J. G. Anchoring of Silver Nanoparticles on Graphitic Carbon Nitride Sheets for the Synergistic Catalytic Reduction of 4-nitrophenol. *Chemosphere* **2017**, *172*, 147-154.

[5] Wu, K. L.; Wei, X. W.; Zhou, X. M.; Wu, D. H.; Liu, X. W.; Ye, Y.; Wang, Q. $NiCo_2$ Alloys: Controllable Synthesis, Magnetic Properties, and Catalytic Applications in Reduction of 4-Nitrophenol. *J. Phys. Chem. C* **2011**, *115*, 16268-16274.

[6] Ji, Z. Y.; Shen, X. P.; Zhu, G. X.; Zhou, H.; Yuan, A. H. Reduced Graphene Oxide/Nickel Nanocomposites: Facile Synthesis, Magnetic and Catalytic Properties. *J. Mater. Chem.* **2012**, *22*, 3471-3477.

[7] Kohantorabi, M.; Gholami, M. R. Kinetic Analysis of the Reduction of 4‑Nitrophenol Catalyzed by CeO_2 Nanorods-Supported CuNi Nanoparticles. *Ind. Eng. Chem. Res.* **2017**, *56*, 1159-1167.

[8] Peng, K.; Fu, L. J.; Yang, H. M.; Ouyang, J.; Tang, A. D. Hierarchical MoS_2 Intercalated Clay Hybrid Nanosheets with Enhanced Catalytic Activity. *Nano Res.* **2017**, *10*, 570-583.

[9] Liu, J. Y.; Yan, X. D.; Wang, L. X.; Kong, L. M.; Jian, P. M. Three-Dimensional Nnitrogen-Doped Graphene Foam as Metal-Free Catalyst for the Hydrogenation Reduction of p-nitrophenol. *J. Colloid Interface Sci.* **2017**, *497*, 102-107.